Synthesis and Catalytic Properties of New Metalloporphyrin-Based Porous Organic Framework Materials with Single and…

Article *in* ChemCatChem · June 2016

DOI: 10.1002/cctc.201600462

CITATION
1

READS
28

9 authors, including:

Xiaoqin Zou
Jilin University
36 PUBLICATIONS **858** CITATIONS
SEE PROFILE

Ma Heping
Changchun Institute of Optics, Fine Mechani…
28 PUBLICATIONS **503** CITATIONS
SEE PROFILE

Hao Ren
Chongqing University
77 PUBLICATIONS **2,469** CITATIONS
SEE PROFILE

Feng Zhang
Harbin Normal University
19 PUBLICATIONS **475** CITATIONS
SEE PROFILE

Some of the authors of this publication are also working on these related projects:

porous luminous material View project

ChemPubSoc Europe

DOI: 10.1002/cctc.201600462

CHEMCATCHEM Full Papers

Synthesis and Catalytic Properties of New Metalloporphyrin-Based Porous Organic Framework Materials with Single and Accessible Sites

Shuang Meng,[a] Xiaoqin Zou,*[b] Chuanfang Liu,[b] Heping Ma,[c] Nian Zhao,[a] Hao Ren,[a] Mingjun Jia,[a] Jia Liu,*[a] and Guangshan Zhu[a]

It is a big challenge to homogenize heterogeneous catalysts with molecular catalytic performance. With this target in mind, herein, we describe a facile strategy for direct incorporation of single catalytic sites in 3D open porous aromatic frameworks (PAFs). The synthesis of the PAF (denoted as PAF-76) as well as its derivatives (PAF-76-M, M = Fe, Mn, Zn) was achieved by the use of tetrakis(4-bromophenyl)methane as tetrahedral nodes and tetrakis(4-bromophenyl)porphyrin as planar nodes. The connection of monomers into an extended network of PAF-76 was monitored by ^{13}C NMR and FTIR spectroscopies. The prepared PAF-76s showed 3D porous structures with surface areas of 450–700 $m^2 g^{-1}$, pore volumes of 0.3–0.4 $cm^3 g^{-1}$, and pore sizes around 1.2 nm. The direct incorporation of metalloporphyrin components into the PAF-76-M frameworks has allowed the uniform distribution of metal ionic sites throughout the PAF-76-M particles. The combined merits of isolated metal sites and suitable pore size make PAF-76 a good candidate for heterogeneous catalysis. The catalytic performances of the porphyrin/metalloporphyrin-based active sites in the PAF-76s were evaluated by aerobic oxidation reactions of styrene, which are usually carried out with homogeneous systems. Metal-functionalized PAF-76s (PAF-76-M) exhibit enhanced turnover frequencies for styrene conversion (16.9–50.9 mol mol(M)$^{-1}$ h^{-1}) compared with molecular catalysts (0–35.0 mol mol(M)$^{-1}$ h^{-1}), and improved selectivity toward phenylacetaldehyde (85.7–99%) in contrast to their corresponding monomers (0–75.5%). The robustness of PAF-76 in terms of high thermal stability, good recyclability, and excellent solvent resistance showed that these PAF-76 materials hold great promise for developing heterogeneous catalysts.

Introduction

Porous organic framework materials (POFs), including covalent organic frameworks (COFs), polymers of intrinsic microporosity (PIM), conjugated microporous polymers (CMPs), and porous aromatic frameworks (PAFs), are emerging as a new family of porous solids.[1–4] POFs are composed of light elements linked by covalent bonds (C–C, C–N, C–O, B–O, etc.), resulting in rigid/diversified structures, permanent porosity, high surface areas, high thermal/chemical stability, tunable pore sizes, and low framework density. Owing to these structural features, POFs with adjustable functions have been widely applied in different areas, particularly in materials science, such as for clean energy storage, molecular separations, photoelectric materials, molecular motors, etc.[5–9] Very recently, intensive efforts have been devoted toward developing catalytically active POF materials with potential applications in chemical catalysis.[10,11]

As we know, homogeneous catalysts have the unique properties of high reactivity and selectivity thanks to their molecular nature.[12] Heterogeneous catalysts possess outstanding advantages for the facile separation of the catalyst from the products, and for the possibility of continuous-flow processes either in the gas or liquid phases. A major goal in catalysis is to combine the merits of both homogeneous catalysis and heterogeneous processes to ideally maintain (or even improve) the activity and selectivity of the molecular catalysts as well as to facilitate product recovery and catalysts recycling. To this end, a series of materials, particularly those of porous materials, have been successfully developed.[13–21] POFs as a subclass of porous materials, have been proposed as an excellent candidate for homo/heterogeneous catalysts because of the tunability of their functionalities (either inherited from the employed monomers, or by post-synthesis modifications) and their chemical stability in the reaction media.[22–42] With the challenge of making homogeneous catalysts heterogeneous, we have become interested in the designed synthesis of POF catalysts by direct incorporation of molecular-like active sites in the

[a] S. Meng, N. Zhao, Dr. H. Ren, Prof. Dr. M. Jia, Dr. J. Liu, Prof. Dr. G. Zhu
College of Chemistry
Jilin University
Changchun 130012 (P.R. China)
E-mail: jia@jlu.edu.cn

[b] Prof. Dr. X. Zou, C. Liu
Faculty of Chemistry
Northeast Normal University
Changchun 130024 (P.R. China)
E-mail: xiaoqinzou123@gmail.com

[c] Dr. H. Ma
State Key Laboratory of Luminescence and Applications
Changchun Institute of Optics, Fine Mechanics and Physics
Chinese Academy of Sciences
Changchun 130033 (P.R. China)

Supporting information and the ORCID identification number(s) for the author(s) of this article can be found under http://dx.doi.org/10.1002/cctc.201600462.

open frameworks, and further evaluation of their catalytic performances.

Herein, porphyrin/metalloporphyrin compounds are chosen as monomers in the construction of POFs based on the following considerations:

1) Metalloporphyrins as active centers. Metalloporphyrins are recognized as well-known analogs of the heme cofactor and most metalloenzymes, which have been extensively used as oxidation catalysts in the fine-chemicals syntheses of epoxides, alcohols, ketones, and aldehydes.[43–45]

2) Metalloporphyrins as building blocks. The utilization of metalloporphyrins as rigid building units for constructing stable frameworks can prevent the leaching of metalloporphyrin sites.[27,33,35,46,47]

In addition, the three-dimensional (3D) porous structure renders the active sites isolated from each other, and thus as many active centers as possible are accessible to reactants compared with homogeneous catalysts. Solid-state catalysts guarantee a facile separation of catalysts from products, allowing their long-term use. This concept is exemplified in this study by the targeted synthesis of a new 3D microporous porphyrin-functionalized PAF and its derivatives, denoted as PAF-76 and PAF-76-M (M = Fe, Mn, or Zn, see Scheme 1). Our previously reported strategy[4,5] has shown that 3D structures can be made by judiciously choosing four-node (tetrahedral) shaped monomers (e.g., PAF-1). Accordingly, a three-dimensional network would be expected for PAF-76 because the center carbon atoms of tetrakis(phenyl)methane adopt a sp^3 tetrahedral configuration. An extended 3D network develops between the tetrahedral and planar building units, which is achieved by terminal C–C bond formation between tetrakis(4-bromophenyl)methane and tetrakis(4-bromophenyl)porphyrin through coupling reactions. Most importantly, porosity would be generated as a result of monomer rigidness, allowing full exposure of the metalloporphyrin moieties. For the derivatives, metalloporphyrins (Fe, Mn, Zn) are employed as monomers for the constructions of identical PAF-76 structures (PAF-76-M). Subsequently, all PAF-76s are studied in the aerobic oxidation of styrene, which is a widely known industrial process for the selective oxidation of organic alkenes to aldehydes.

Results and Discussion

Structure determination

The formation of porphyrin-based PAF-76s involves the creation of new C–C bonds between 5,10,15,20-tetrakis-(4-bromophenyl)-porphyrin (TBPP) and tetrakis[4-(4′,4′,5′,5′-tetramethyl-1′,3′,2′-dioxaborolane-phenyl)]methane (TTBPM) by cross-coupling reactions, and the conjugated network results from extensive polymerization with the elimination of small molecules (Scheme 1). For clarifying the linkage of monomers and the microstructure of PAF-76, solid-state ^{13}C NMR spectroscopy is a powerful technique, which was used to examine the carbon

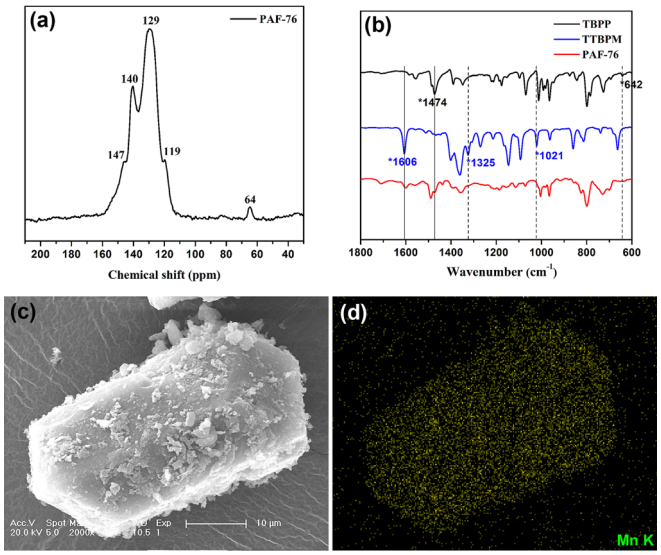

Figure 1. a) ^{13}C solid-state MAS NMR spectrum of the as-synthesized PAF-76, b) FTIR spectra of TBPP and TTBPM reactants and PAF-76 product, c) a representative SEM image, and d) manganese distribution map of PAF-76-Mn.

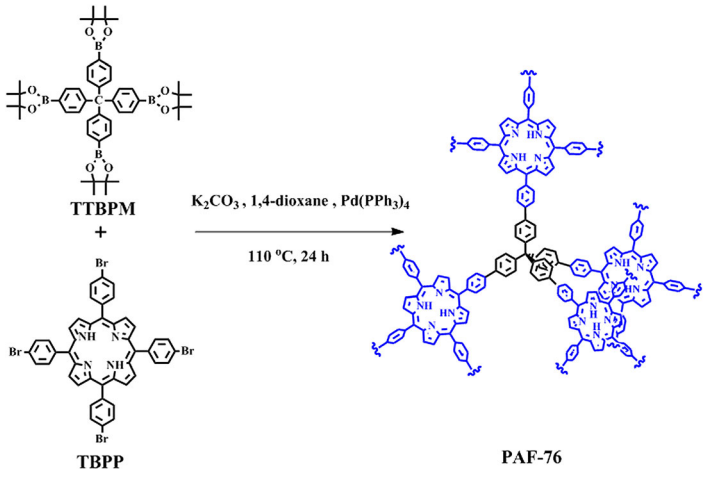

Scheme 1. A representation of the synthesis of PAF-76 employing TTBPM and TBPP reactants.

connectivity of PAF-76. Figure 1a presents the NMR spectrum of the PAF-76 product. As shown in Figure 1a, a carbon signal at 64 ppm is detected, which is assigned to the center carbon with a tetrahedral configuration. Additionally, a shoulder peak at 147 ppm is observed, which is attributed to the carbon atoms in the pyrrole ring. It can be found that the carbon signals from boron esters disappear (Figure S1a in the Supporting Information), suggesting that the boron groups are cleaved off from the monomers when the cross-coupling reaction takes place at 383 K (110 °C). Moreover, carbon signals from the benzene ring merge together to form three easily distinguished peaks around 119 ppm, 129 ppm, 140 ppm with the concurrent disappearances of C–B and C–Br peaks at 127 ppm (Figure S1a) and 125 ppm (Figure S1b). The peaks merging and broad-

ening is due to the connection of TBPP and TTBPM monomers through C–C bonds with consequent formation of a more conjugated structure of PAF-76. Further, the PAF-76 structure was characterized by infrared (IR) spectroscopy, and the result is displayed in Figure 1b. The band corresponding to C–Br vibrations at 642 cm^{-1} (Figure 1b) in PAF-76 vanishes into the background (red line), indicating that the C–Br bond is replaced by a C–C bond; which is in good agreement with the NMR results. The C–B and B–O associated bands at 1021 cm^{-1} and 1325 cm^{-1}, respectively, were not observable in the PAF-76 sample, suggesting that the boron ester group was detached from the carbon atom of the benzene ring during the cross-coupling reaction, which is also consistent with the NMR observations.

Clear bands at 1606 cm^{-1} and 1474 cm^{-1} are detected, which suggest that the main backbone of the phenyl and pyrrole rings is preserved in PAF-76. A similar NMR profile for PAF-76-Zn suggests that the PAF-76 derivatives (Figure S2 in the Supporting Information) possess the same structure as that of PAF-76, which is further verified by the IR spectra (Figure S3 in the Supporting Information). Elemental analysis data in Table S1 (in the Supporting Information) shows the chemical composition of C, H, and N for PAF-76 with trace Pd (~0.5 wt%), affording a molecular formula of $C_{69}H_{42}N_4$, which is in agreement with the structure in Scheme 1. Based on the results from NMR, IR, and elemental analyses, it can be concluded that an extended network of PAF-76 is constructed from TBPP and TTBPM by coupling reactions.

The morphology and element distribution of PAF-76s were studied by scanning electron microscopy (SEM). A representative SEM image of the PAF-76-Mn sample shows a hexagonal-shaped bulk particle around tens of micrometers in size with small-sized aggregates (Figure 1c). Figure 1d shows the distribution map of manganese element in one of the PAF-76-Mn particles, measured by energy-dispersive X-ray spectroscopy (EDS). The EDS profile in Figure 1d reveals that manganese is mainly located within the PAF-76-Mn particle and is homogeneously distributed throughout the polymer. The uniform distribution of metal ions is also observed in its analogs (Fe and Zn derivatives, Figure S4 in the Supporting Information). The quantitative determination of metal contents in PAF-76-M was done by chemical analysis by inductively coupled plasma optical emission spectroscopy (ICP-OES). As shown from the metal/porphyrin ring ratio of approximately 0.9 in Table S2 (in the Supporting Information), almost a stoichiometric amount of metal ions are incorporated into the porphyrin rings in PAF-76s. Consequently, each metal ion is confined within one porphyrin ring, which favors the isolated and single metal centers. A similar metal/porphyrin ratio (≈0.8) of the polymer to the corresponding monomers (≈0.9) sheds light on the high stability of the metalloporphyrin components in the solvent (i.e., dioxane). In addition to the chemical stability, the thermal stability was also examined by thermogravimetric analysis (TGA). A small weight loss of 2–6% is observed before 300 °C (Figure S5 in the Supporting Information), attributed to solvent release (e.g., methanol). TGA results confirm that PAF-76s exhibit relatively high thermal stability (up to 300 °C), which permits their subsequent catalysis applications.

The oxidation states of the metal species in PAF-76-M were probed by X-ray photoelectron spectroscopy (XPS). Figure 2 shows the XPS spectra for PAF-76-Fe, PAF-76-Mn, and PAF-76-Zn. As shown in Figure 2a, the Fe 2p region has significantly split spin–orbit components of Fe $2p_{3/2}$ and Fe $2p_{1/2}$. The Fe $2p_{3/2}$ spectrum of PAF-76-Fe displays a peak maximum near 710.8 eV and a satellite peak at 718.3 eV, characteristic of the Fe^{III} state. For PAF-76-Mn, the Mn 2p spectrum contains a Mn $2P_{3/2}$ peak at 642.3 eV and Mn $2p_{1/2}$ peak at 654.1 eV (Figure 2b). These features show that the Mn species in PAF-76-Mn possess a high valence of Mn^{IV}.[48] The reason for the high oxidation state of iron and manganese is the likelihood of additional oxidation of Fe^{II} and Mn^{II} to the respective Fe^{III} and Mn^{IV} species with an exposure of PAF-76-Fe and PAF-76-Mn to air.

The permanent porosity and specific surface area of the PAF-76s were determined by nitrogen physical sorption at 77 K. Figure 3a shows the N_2 adsorption–desorption isotherms for PAF-76s. A steep uptake at low relative pressures followed by a steady increase in the adsorption branch was recorded in the sorption isotherms of PAF-76 materials, typical for microporous materials. The possible reason for the observed hysteresis could be the capillary condensation of N_2 in some bottle-shaped pores formed by interpenetrated polymerization or inter-particle voids formed by aggregation of similar-in-size small particles as seen by SEM (Figure 1c). The specific Brun-

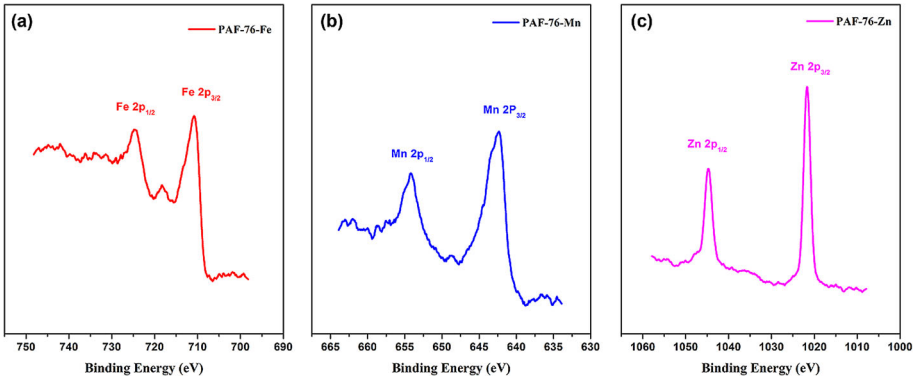

Figure 2. XPS spectra of a) Fe 2p, b) Mn 2p, and c) Zn 2p signals in PAF-76-Fe, PAF-76-Mn, and PAF-76-Zn, respectively.

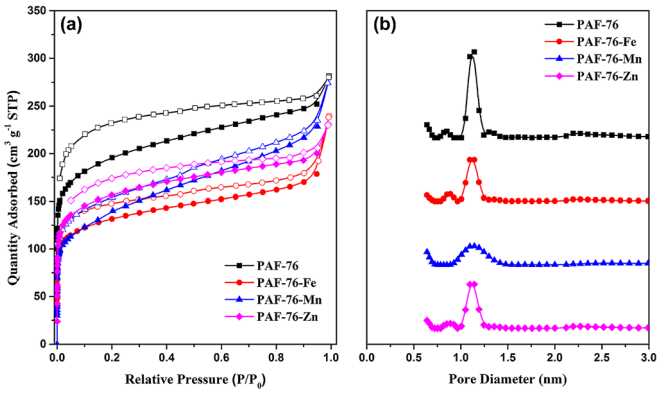

Figure 3. a) N_2 adsorption isotherms at 77 K and b) the DFT-derived pore size distribution curves of PAF-76, PAF-76-Fe, PAF-76-Mn, and PAF-76-Zn.

auer–Emmet–Teller surface areas (S_{BET}) and pore volumes are summarized in Table S3 (in the Supporting Information). The S_{BET} and pore volumes of all PAF-76s materials are in the ranges 450–700 $m^2 g^{-1}$ and 0.3–0.4 $cm^3 g^{-1}$, respectively. These values correspond to a highly porous material, which is in agreement with our synthesis concept by using tetrahedral and planar building blocks (Scheme 1). Pore size distribution curves are presented in Figure 3b. Based on the non-local density functional theory (NL-DFT), the pore size distribution (PSD) of PAF-76 exhibits a dominant pore diameter of 1.2 nm, and the PSD of PAF-76 metal derivatives exhibit similar dominant ones of 1.1–1.2 nm (Figure 3b and Table S3), suggesting that PAF-76 and PAF-76-M have the same porous structure. More importantly, the porous characteristics of PAF-76-Mn, PAF-76-Fe, and PAF-76-Zn would have great benefits for high accessibility of the metal sites as well as fast mass transport.

Catalytic properties

To assess the catalytic properties, PAF-76s with metalloporphyrin moieties in the framework were investigated for the aerobic oxidation reaction of styrene as a substrate, which is an important chemical feedstock for alkenes conversions.[47] The aerobic oxidation reactions were performed by using 1 mmol of styrene substrate and 3 mmol of isobutyraldehyde co-reductant in 10 mL of 1,2-dichloroethane solvent ($C_2H_4Cl_2$ used to completely dissolve metalloporphyrin monomers) with 10 mg of PAF-76 catalysts for 2 h under ambient pressure (1 atm) and temperature of 353 K. The catalytic results of conversion, turnover frequency, and selectivity for PAF-76s and their corresponding homogenous metalloporphyrin catalysts are summarized in Table 1. The PAF-76 catalysts exhibit excellent selectivities for phenylacetaldehyde (85–99%, entries 1, 3, 5, 7). No 2-phenyloxirane side product was observed, and only a small amount of benzaldehyde (< 14.3%) was found after 2 h reaction over PAF-76-M catalysts (entries 3, 5, 7). The formation of trace benzaldehyde product is probably due to over oxidation. The relatively small conversion of 27.4% with PAF-76 might come from styrene activation on trace Pd metals or defect sites. Interestingly, the respective turnover frequencies of 40.4, 41.5, 13.5 mmol $g_{cat}^{-1} h^{-1}$ are observed with PAF-76-Fe, PAF-76-Mn, PAF-76-Zn after a reaction time of 2 h (entries 3, 5, 7 in Table 1). The catalytic performance is quite reproducible as seen from similar conversions for two independent runs (Figure S6 in the Supporting Information). Under the same conditions, the metalloporphyrin monomers afforded a bit lower substrate conversion rate with values of 32.0, 31.5, and 0 mmol $g_{cat}^{-1} h^{-1}$ (entries 4, 6, 8 in Table 1). The above experimental results clearly demonstrate that PAF-76 catalysts performed equally as well (or even outperformed) as their homogeneous metalloporphyrin analogs. The enhancements in terms of turnover frequency (> 26%) and selectivity (> 18%) suggest that the micro-environment plays a great role in sty-

Table 1. Catalytic data for styrene oxidation over PAF-76 and its metallo-derivative PAFs as well as their corresponding porphyrin-based monomers.

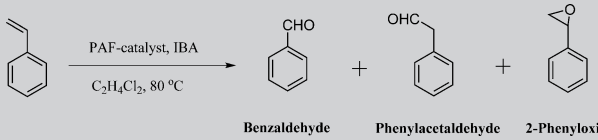

Benzaldehyde Phenylacetaldehyde 2-Phenyloxirane

Entry	Conversion [%][a]	Selectivity [%][b]			Turnover frequency[c]	
		Benzaldehyde	Phenylacetaldehyde	2-Phenyloxirane	[mmol $g_{cat}^{-1} h^{-1}$]	[mol mol(M)$^{-1} h^{-1}$]
PAF-76	27.4	0	> 99	0	13.5	–
TBPP	0	0	0	0	0	–
PAF-76-Fe	80.7	10.7	89.3	0	40.4	48.3
Fe-TBPP	64.1	24.5	75.5	0	32.0	35.0
PAF-76-Mn	83.7	14.3	85.7	0	41.5	50.9
Mn-TBPP	63.8	33.3	66.7	0	31.5	34.1
PAF-76-Zn	27.2	0	> 99	0	13.5	16.9
Zn-TBPP	0	0	0	0	0	0

[a] Reaction conditions: 1 mmol of substrate, 3 mmol of isobutyraldehyde (IBA), 10 mg of catalyst, 10 mL of 1,2-dichloroethane ($C_2H_4Cl_2$), 1 atm, and 353 K (80 °C) for 2 h. [b] Conversion and selectivity determined by GC by using benzene as an internal standard. [c] Turnover frequency is expressed as the consumption (conversion) of styrene at 2 h per time in terms of catalyst weight and moles of metal.

rene conversion as a result of the enrichment of reactants in the micropores. Note that the turnover frequencies of PAF-76-Fe and PAF-76-Mn (48.3 and 50.9 mol mol(M)$^{-1}$ h^{-1}, respectively) are almost three times the value of that over PAF-76-Zn (16.9 mol mol(M)$^{-1}$ h^{-1}). These enhancements with PAF-76-Fe and PAF-76-Mn catalysts can be interpreted by the fact that there are empty 3d orbits accepting the electrons from the reactants or co-reactant in PAF-76-Fe and PAF-76-Mn because Fe^{III} and Mn^{IV} adopt $3d^5$ and $3d^3$ electron configurations. However, in the case of PAF-76-Zn, no empty 3d orbits are available in Zn^{II} owing to its $3d^{10}$ configuration; that is, the poor electron accepting ability results in low turnover frequency of styrene conversion. This experimental result demonstrates that metal centers with unsaturated orbits are of vital importance in styrene conversion, as well as shedding light on the electron-based mechanism for the oxidation of styrene to phenylacetaldehyde. This conclusion can be supplementary supported by the results from homogeneous catalysts, as evident from the turnover frequencies of, respectively, 35.0 and 34.1 mol mol(M)$^{-1}$ h^{-1} with Fe-TBPP and Mn-TBPP (entries 4 and 6 in Table 1) in contrast to undetectable styrene conversion on Zn-TBPP (entry 8, Table 1).

To study the mechanistic behavior and also to identify the active species formed in the oxidation of styrene, a small amount of free radical scavenger, 2,6-di-*tert*-butylphenol (1 mmol), was added, and the catalytic activity with PAF-76-Mn was examined. With the same reaction parameters specified in Table 1, the turnover frequency of styrene conversion is significantly decreased (4.5 mol mol(M)$^{-1}$ h^{-1}) with a small conversion of 7.4% after 2 h in comparison to that measured without addition of radical scavenger (entry 5, Table 1). This result, along with the data in Table 1, confirms that free-radical-type species occurs during the reaction. To further shed light on the involvement of radicals in this oxidation, a reference experiment in the absence of isobutyraldehyde was carried out under the same reaction circumstances described in Table 1. A relatively small conversion of 5.3% for styrene is found, suggesting that styrene consumption is initiated by isobutyraldehyde radicals. Based on the results in Table 1 and from the two control experiments, a tentative reaction mechanism for the aerobic oxidation of styrene is proposed, which is exemplified by the PAF-76-Mn catalyst as shown in Scheme 2. Upon interaction of isobutyraldehyde with PAF-76-Mn, the isobutyraldehyde radical is generated by hydrogen abstraction from a sacrificial co-reductant of isobutyraldehyde,[49] and intermediate Mn species **2** is concurrently formed by electron and hydrogen transfers.[50]

The produced radical is rapidly captured by compound **2** and subsequently converted to a complex radical of **3**.[51,52] The

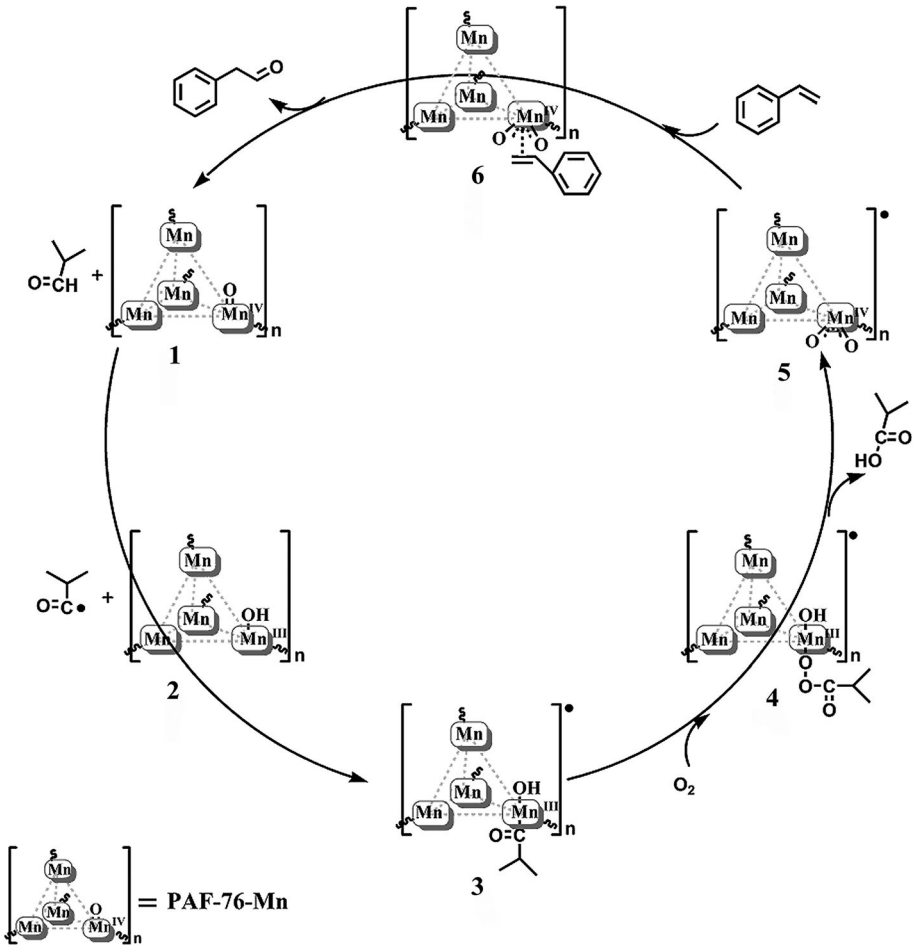

Scheme 2. Possible mechanism for the aerobic oxidation of styrene to its corresponding aldehyde catalyzed by PAF-76-Mn in the presence of molecular oxygen and isobutyraldehyde.

activation of molecular oxygen occurs on **3** through the formation of active species **4**.[53] The complex **4** is most likely decomposed to form metal-peroxo species of **5**, with concerted release of isobutyric acid.[54] The cleavage of C=C bonds takes place by an interaction of styrene with complex **5**. Phenylacetaldehyde is yielded by the isomerization/rearrangement of the styrene oxide intermediate inside complex **6**, and the side product of benzaldehyde may be produced by the deep oxidation of the formed oxide species in **6**.[55,56] Meanwhile, Mn species in PAF-76-Mn is regenerated to the initial state of **1** after the whole catalytic circle.

More information on the catalytic properties of PAF-76-M can be obtained from the oxidation of styrene derivatives, which is exemplified by methylphenylene and chlorostyrene. Figure 4 shows the oxidation results of 4-methylphenylene and

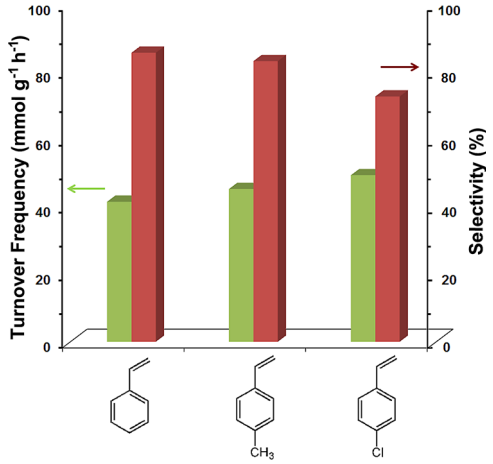

Figure 4. Turnover frequency of styrene, 4-methylphenylene, and 4-chlorostyrene conversion, and the respective selectivity for phenylacetaldehyde, 4-methylphenylacetaldehyde, and 4-chlorophenylacetaldehyde products, over PAF-76-Mn catalyst.

4-chlorostyrene over PAF-76-Mn catalyst. When 4-methylphenylene is used as the substrate, its oxidation over PAF-76-Mn proceeds at a frequency of 45.3 mmol $g_{cat}^{-1} h^{-1}$ and the major product is 4-methylphenylacetaldehyde with a selectivity of 83.2%. In the case of 4-chlorostyrene oxidation, PAF-76-Mn displays a turnover frequency of 49.4 mmol $g_{cat}^{-1} h^{-1}$ for 4-chlorostyrene conversion, with a selectivity of 72.8% for 4-chlorophenylacetaldehyde. As shown in Figure 4, similar results for 4-methylphenylene and 4-chlorostyrene substrates to that of styrene oxidation are observed in terms of turnover frequency (41.5 mmol $g_{cat}^{-1} h^{-1}$ for styrene conversion) and product selectivities for aldehydes (85.7% for phenylacetaldehyde). This observation indicates that the presence of the *para*-methyl and -chloro functional groups in the substrates does not significantly affect the oxidative conversions of styrenic compounds. This finding also supports the radical-mediated mechanism of styrene oxidation because an electron donor or acceptor on the styrene molecules has little influence on C=C bond cleavage (Scheme 2).

As metalloporphyrins are expensive organocatalysts, their stability and recyclability is another important index. To address the recyclability of PAF-76 catalysts, the multiple repeated reactions were carried out with PAF-76-Mn. As expected, it is found that the turnover frequency of styrene conversion is well retained around 45 mmol $g_{cat}^{-1} h^{-1}$, and the selectivity for phenylacetaldehyde (~85%) is preserved as well after recycling for five times (Figure 5). These results confirm that PAF-76 catalysts possess excellent recyclability. Almost all the catalyst is recycled after each run by separating the solid from the liquid with weight losses of <7%. The data from inductively coupled plasma optical emission spectroscopy (ICP-OES) shows that the concentration of Mn species in the supernatant after each run is beyond our ICP detection limit (40 ppb). The small loss in catalyst weight and negligible Mn leaching prove the high stability of PAF-76 catalysts. Additionally, catalytic tests of PAF-76-Mn were also performed in different solvents (1,2-dichloroethane, acetonitrile, and tetrahydrofuran), and the results are summarized in Table S4 (in the Supporting Information). The similar turnover frequency of styrene conversion ($\approx$41 mmol $g_{cat}^{-1} h^{-1}$) and selectivity for phenylacetaldehyde (~80%) validate the high chemical robustness of PAF-76 catalysts.

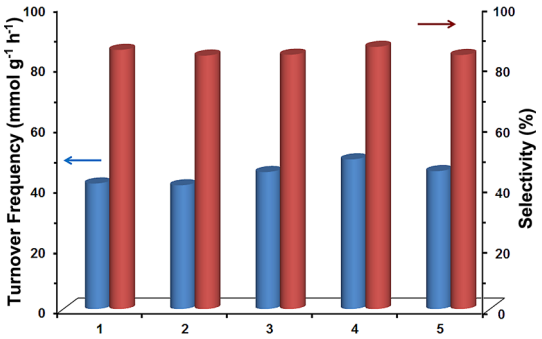

Figure 5. Turnover frequency of styrene conversion and the selectivity for phenylacetaldehyde as a function of number of recycling tests.

Conclusions

In summary, we have developed a new synthesis strategy for introducing functionalities into 3D microporous aromatic frameworks (PAF-76s) by cross-coupling of porphyrin/metalloporphyrin-based monomers and tetrakis(4-bromophenyl)methane. As-prepared PAF-76 possesses a conjugated network linked by intensive and newly created C–C bonds between two building units, the structure of which has been verified by NMR and IR measurements. N_2 adsorption characterization has revealed that PAF-76s exhibit permanent porosity, high surface areas, as well as a molecular-level pore sizes. The direct incorporation approach favors uniform distribution of metal ions in the PAF backbone, which has been demonstrated by energy-dispersive X-ray spectroscopy and elemental analysis. Metalloporphyrin-functionalized PAF-76s have been further explored as heterogeneous catalysts for the selective oxidation of styrene to phenylacetaldehyde. Catalytic results have revealed that the PAF-76 catalysts show superior catalytic performance

including high turnover frequency of styrene conversion and high selectivity for phenylacetaldehyde product, which is due to the single and highly accessible metal sites in the frameworks and an enrichment of reactants in the micropores. The radical catalytic mechanism for the aerobic oxidation of styrene has been elucidated on PAF-76-Mn, which included a sequence of radical generation and stabilization on the Mn center, the formation of metal-peroxo intermediates assisted by molecular oxygen, and C=C bond cleavage on the active Mn–O sites with concurrent formation of phenylacetaldehyde. In addition, as-synthesized PAF-76 catalysts have shown high thermal stability, good recyclability, and excellent robustness toward solvents. This study may provide us with some guidelines for the designed synthesis of efficient porous heterogeneous catalysts, and other new endeavors that are being explored in our group.

Experimental Section

Synthesis of monomers

The synthesis of tetrakis[4-(4′,4′,5′,5′-tetramethyl-1′,3′,2′-dioxaborolane-phenyl)]methane (TTBPM) was conducted according to an established procedure.[57] Typically, tetrakis(4-bromophenyl)methane (1.3 g, 2.0 mmol) was dissolved in dry ethyl ether (35 mL) and cooled to 203 K. Under nitrogen, butyllithium/hexane solution (6.0 mL of 2.5 M) was added slowly in the above solution with stirring. After warming to room temperature, another solution of trimethyl borate (3.2 g, 31 mmol) in dry ethyl ether (30 mL) was added and stirred for 1 h. The ether was then removed under vacuum at room temperature. The product was collected by filtration, washed with water, and dried in vacuum. The product (1 g, 2 mmol) and pinacol (1.1 g, 9.6 mmol) were added to ethyl acetate (30 mL), and this reaction mixture was heated at reflux for 24 h. After cooling down to room temperature, the crude product was collected by filtration, washed with ethanol, and then dried in vacuum at room temperature. ^{1}H NMR (400 MHz, $CDCl_3$) of TTBPM: $\delta_H = 7.6$ (d, $J = 11.2$ Hz, 8H), 7.3 (d, $J = 10.4$ Hz, 8H), 1.3 ppm (s, 48H).

The preparation of 5,10,15,20-tetrakis-(4-bromophenyl)-porphyrin (TBPP) was carried out as follows: 4-bromobenzaldehyde (1.5 g, 8.46 mmol), pyrrole (0.6 mL, 8.46 mmol), and CH_2Cl_2 (850 mL) solvent were added to a foil-covered 2.0 L three-necked flask equipped with a reflux condenser, a magnetic stirrer, and a N_2 inlet. The reaction mixture was first stirred for 15 min at room temperature, and then $BF_3{\cdot}OEt_2$ (105 μL, 0.85 mmol) was added. After 2 h, *p*-chloranil (1.56 g, 6.37 mmol) was added, and the reaction mixture was heated to reflux for 2 h. The obtained liquid mixture after reaction was evaporated to a volume of 50–100 mL, followed by further purification by using silica gel.[58] ^{1}H NMR (400 MHz, $CDCl_3$) of TBPP: $\delta_H = -2.9$ (s, 2H), 7.8 (d, $J = 11.2$ Hz, 8H), 8.0 (d, $J = 11.2$ Hz, 8H), 8.8 ppm (s, 8H).

The preparations of Fe-TBPP, Mn-TBPP and Zn-TBPP were done by first mixing TBPP (900 mg, 0.97 mmol) and the metal source (900 mg, 7.14 mmol $FeCl_2$; or 900 mg, 7.14 mmol $MnCl_2$; or 970 mg, 7.14 mmol $ZnCl_2$) in DMF (100 mL), with subsequent reflux for 5 h under an argon atmosphere. The reaction mixture was cooled to room temperature, and then DMF was evaporated under vacuum. The crude product was purified by silica gel column chromatography.

The chemicals of tetrakis(4-bromophenyl)methane, butyllithium, trimethyl borate, pinacol, 4-bromobenzaldehyde, pyrrole, $BF_3{\cdot}OEt_2$, *p*-chloranil, $FeCl_2$, $MnCl_2$, $ZnCl_2$, K_2CO_3, DMF, ethyl ether, hexane, ethyl acetate, ethanol, CH_2Cl_2, 1,4-dioxane, tetrakis(triphenylphosphine)-palladium(0) were used as received without any further purification.

Synthesis of PAF-76

5,10,15,20-Tetrakis-(4-bromophenyl)-porphyrin (204 mg, 0.2 mmol, abbreviated as TBPP) and tetrakis[4-(4′,4′,5′,5′-tetramethyl-1′,3′,2′-dioxaborolane-phenyl)]methane (165 mg, 0.2 mmol, abbreviated as TTBPM) were introduced into a dry 50 mL two-necked flask with a condenser and a magnetic stirring bar inside the flask. After degassing with argon, 1,4-dioxane (20 mL), anhydrous K_2CO_3 (220 mg) and tetrakis(triphenylphosphine)palladium(0) as a catalyst (23 mg, 20 μmol, abbreviated as $Pd(PPh_3)_4$) were added into the flask, and then the mixture was heated to 383 K for 24 h under an inert atmosphere. After cooling to room temperature, the crude product was collected by filtration, and then washed with ethanol and methanol. Further purification of PAF-76 was carried out by Soxhlet extraction with tetrahydrofuran (THF) and methanol for 24 h. The product was dried in vacuum at 393 K to give PAF-76 as a purple powder. The syntheses of PAF-76-Fe, PAF-76-Mn and PAF-76-Zn were performed by using the same procedure but by substituting TBPP with Fe-TBPP, Mn-TBPP, or Zn-TBPP, respectively.

Characterizations

The solid-state cross-polarization magic angle spinning ^{13}C nuclear magnetic resonance spectra (CP-MAS NMR) were collected with a Bruker Avance III 400 MHz solid-state NMR spectrometer at a MAS rate of 5 kHz. Fourier transform infrared spectra (FTIR) were measured by using a Nicolet Impact 410 FTIR spectrometer at room temperature in the range 400–4000 cm^{-1}, with potassium bromide pellets. Field emission scanning electron microscope (FE-SEM) images were inspected with a Hitachi S-4800 with energy-dispersive X-ray spectroscopy (EDS). X-ray photoelectron spectroscopy (XPS) measurements were performed with an ESCALAB 250 spectrometer. The nitrogen sorption measurements were carried out with a Quantachrome Autosorb iQ2 analyzer. Prior to the measurements, the samples were degassed at 393 K for 24 h. N_2 adsorption isotherms were recorded at 77 K by using ultra-high-purity grade N_2 (99.999%). The thermogravimetric analysis (TGA) was performed by using a Netzch Sta 449c thermal analyzer system at a heating rate of 10 K min^{-1} in an air atmosphere. The metal contents of Fe, Mn, and Zn in the monomers and PAF-76 polymers were analyzed by inductively coupled plasma optical emission spectrometer (ICP-OES, PerkinElmer Optima 3300DV), and the C, H, N contents were determined by using a PerkinElmer 2400 Series II CHNS/O analyzer.

Catalytic tests

Styrene oxidations were performed on the monomers (TBPP, Fe-TBPP, Mn-TBPP, Zn-TBPP) and PAF-76 samples in a batch glass reactor. The catalyst (10 mg) was loaded into a reactant solution containing styrene (1 mmol, 0.12 mL), isobutyraldehyde (3 mmol, 0.27 mL), benzene (63.7 mg) as an internal standard, and 1,2-dichloroethane (10 mL) solvent in a 50 mL three-necked round-bottom flask. An O_2 stream (5 mL min^{-1}, 1.0 atm, 99.999%) was introduced into the reactor from one inlet, and the reactor was further heated to 353 K (80 °C). The reaction process was monitored by taking one sample every 30 min by using a syringe from another outlet. Reactant and product concentrations were measured by

using gas chromatography (BRUKER 450-GC) with a capillary column (GCBP; 30 m×0.53 mm, 1.0 μm film thickness) connected to a flame ionization detector. The turnover frequency after 2 h reaction was defined as the number of molecules (mol) converted per time (h) normalized by catalyst weight (g) or the number of metal atoms (mol).

Acknowledgments

We are grateful to the financial support from the National Basic Research Program of China (973 Program, grant nos. 2012CB821700, 2014CB931800), National Natural Science Foundation of China (NSFC grant nos. 21501024, 21401069), and Major International (Regional) Joint Research Project of NSFC (grant no. 21120102034).

Keywords: heterogeneous catalysis · metalloporphyrin single sites · porous aromatic frameworks · selective styrene oxidation · superior catalytic performance

[1] A. P. Côté, A. I. Benin, N. W. Ockwig, M. O'Keeffe, A. J. Matzger, O. M. Yaghi, *Science* **2005**, *310*, 1166 – 1170.
[2] N. B. McKeown, P. M. Budd, *Macromolecules* **2010**, *43*, 5163 – 5176.
[3] A. I. Cooper, *Adv. Mater.* **2009**, *21*, 1291 – 1295.
[4] T. Ben, H. Ren, S. Q. Ma, D. P. Cao, J. H. Lan, X. F. Jing, W. C. Wang, J. Xu, F. Deng, J. M. Simmons, S. L. Qiu, G. S. Zhu, *Angew. Chem. Int. Ed.* **2009**, *48*, 9457 – 9460; *Angew. Chem.* **2009**, *121*, 9621 – 9624.
[5] X. Q. Zou, H. Ren, G. S. Zhu, *Chem. Commun.* **2013**, *49*, 3925 – 3936.
[6] F. Vilela, K. Zhang, M. Antonietti, *Energy Environ. Sci.* **2012**, *5*, 7819 – 7832.
[7] Y. H. Xu, S. B. Jin, H. Xu, A. Nagai, D. L. Jiang, *Chem. Soc. Rev.* **2013**, *42*, 8012 – 8031.
[8] M. D. Guiver, Y. M. Lee, *Science* **2013**, *339*, 284 – 285.
[9] S. Lin, C. S. Diercks, Y. B. Zhang, N. Kornienko, E. M. Nichols, Y. B. Zhao, A. R. Paris, D. Kim, P. D. Yang, O. M. Yaghi, C. J. Chang, *Science* **2015**, *349*, 1208 – 1213.
[10] P. Kaur, J. T. Hupp, S. T. Nguyen, *ACS Catal.* **2011**, *1*, 819 – 835.
[11] Q. Sun, Z. F. Dai, X. J. Meng, L. Wang, F. S. Xiao, *ACS Catal.* **2015**, *5*, 4556 – 4567.
[12] M. P. de Almeida, S. A. C. Carabineiro, *ChemCatChem* **2012**, *4*, 18 – 29.
[13] L. Y. Li, Z. L. Chen, H. Zhong, R. H. Wang, *Chem. Eur. J.* **2014**, *20*, 3050 – 3060.
[14] Q. Sun, X. J. Meng, X. Liu, X. M. Zhang, Y. Yang, Q. H. Yang, F. S. Xiao, *Chem. Commun.* **2012**, *48*, 10505 – 10507.
[15] L. Stegbauer, K. Schwinghammer, B. V. Lotsch, *Chem. Sci.* **2014**, *5*, 2789 – 2793.
[16] R. Palkovits, M. Antonietti, P. Kuhn, A. Thomas, F. Schüth, *Angew. Chem. Int. Ed.* **2009**, *48*, 6909 – 6912; *Angew. Chem.* **2009**, *121*, 7042 – 7045.
[17] Z. G. Xie, C. Wang, K. E. deKrafft, W. B. Lin, *J. Am. Chem. Soc.* **2011**, *133*, 2056 – 2059.
[18] Y. Z. Lei, L. J. Wu, X. F. Zhang, H. Mei, Y. L. Gu, G. X. Li, *J. Mol. Catal. A* **2015**, *398*, 164 – 169.
[19] E. Verde-Sesto, M. Pintado-Sierra, A. Corma, E. M. Maya, J. G. de La Campa, M. Iglesias, F. Sánchez, *Chem. Eur. J.* **2014**, *20*, 5111 – 5120.
[20] J. Thote, H. B. Aiyappa, A. Deshpande, D. D. Díaz, S. Kurungot, R. Banerjee, *Chem. Eur. J.* **2014**, *20*, 15961 – 15965.
[21] N. Kang, J. H. Park, K. C. Ko, J. Chun, E. Kim, H. W. Shin, S. M. Lee, H. J. Kim, T. K. Ahn, J. Y. Lee, S. U. Son, *Angew. Chem. Int. Ed.* **2013**, *52*, 6228 – 6232; *Angew. Chem.* **2013**, *125*, 6348 – 6352.
[22] X. Wang, S. M. Lu, J. Li, Y. Liu, C. Li, *Catal. Sci. Technol.* **2015**, *5*, 2585 – 2589.
[23] E. Merino, E. Verde-Sesto, E. M. Maya, M. Iglesias, F. Sánchez, A. Corma, *Chem. Mater.* **2013**, *25*, 981 – 988.
[24] S. J. Kraft, R. H. Sánchez, A. S. Hock, *ACS Catal.* **2013**, *3*, 826 – 830.
[25] H. J. Mackintosh, P. M. Budd, N. B. McKeown, *J. Mater. Chem.* **2008**, *18*, 573 – 578.
[26] Q. Sun, Z. F. Dai, X. L. Liu, N. Sheng, F. Deng, X. J. Meng, F. S. Xiao, *J. Am. Chem. Soc.* **2015**, *137*, 5204 – 5209.
[27] A. M. Shultz, O. K. Farha, J. T. Hupp, S. T. Nguyen, *Chem. Sci.* **2011**, *2*, 686 – 689.
[28] F. Wang, J. Mielby, F. H. Richter, G. H. Wang, G. Prieto, T. Kasama, C. Weidenthaler, H. J. Bongard, S. Kegnæs, A. Fürstner, F. Schüth, *Angew. Chem. Int. Ed.* **2014**, *53*, 8645 – 8648; *Angew. Chem.* **2014**, *126*, 8789 – 8792.
[29] Q. R. Fang, S. Gu, J. Zheng, Z. B. Zhuang, S. L. Qiu, Y. S. Yan, *Angew. Chem. Int. Ed.* **2014**, *53*, 2878 – 2882; *Angew. Chem.* **2014**, *126*, 2922 – 2926.
[30] X. S. Wang, M. Chrzanowski, D. Q. Yuan, B. S. Sweeting, S. Q. Ma, *Chem. Mater.* **2014**, *26*, 1639 – 1644.
[31] P. Zhang, Z. H. Weng, J. Guo, C. C. Wang, *Chem. Mater.* **2011**, *23*, 5243 – 5249.
[32] S. Y. Ding, J. Gao, Q. Wang, Y. Zhang, W. G. Song, C. Y. Su, W. Wang, *J. Am. Chem. Soc.* **2011**, *133*, 19816 – 19822.
[33] B. Saha, D. Gupta, M. M. Abu-Omar, A. Modak, A. Bhaumik, *J. Catal.* **2013**, *299*, 316 – 320.
[34] Y. G. Zhang, S. N. Riduan, J. Y. Ying, *Chem. Eur. J.* **2009**, *15*, 1077 – 1081.
[35] L. Chen, Y. Yang, D. L. Jiang, *J. Am. Chem. Soc.* **2010**, *132*, 9138 – 9143.
[36] R. K. Totten, Y. S. Kim, M. H. Weston, O. K. Farha, J. T. Hupp, S. T. Nguyen, *J. Am. Chem. Soc.* **2013**, *135*, 11720 – 11723.
[37] J. X. Jiang, C. Wang, A. Laybourn, T. Hasell, R. Clowes, Y. Z. Khimyak, J. L. Xiao, S. J. Higgins, D. J. Adams, A. I. Cooper, *Angew. Chem. Int. Ed.* **2011**, *50*, 1072 – 1075; *Angew. Chem.* **2011**, *123*, 1104 – 1107.
[38] B. Y. Li, Z. H. Guan, W. Wang, X. J. Yang, J. L. Hu, B. Tan, T. Li, *Adv. Mater.* **2012**, *24*, 3390 – 3395.
[39] P. Puthiaraj, K. Pitchumani, *Green Chem.* **2014**, *16*, 4223 – 4233.
[40] K. Zhang, D. Kopetzki, P. H. Seeberger, M. Antonietti, F. Vilela, *Angew. Chem. Int. Ed.* **2013**, *52*, 1432 – 1436; *Angew. Chem.* **2013**, *125*, 1472 – 1476.
[41] J. X. Jiang, Y. Y. Li, X. F. Wu, J. L. Xiao, D. J. Adams, A. I. Cooper, *Macromolecules* **2013**, *46*, 8779 – 8783.
[42] C. E. Chan-Thaw, A. Villa, P. Katekomol, D. S. Su, A. Thomas, L. Prati, *Nano Lett.* **2010**, *10*, 537 – 541.
[43] W. J. Zhang, P. P. Jiang, Y. Wang, J. Zhang, P. B. Zhang, *Appl. Catal. A* **2015**, *489*, 117 – 122.
[44] C. Zou, M. Zhao, C. D. Wu, *Catal. Commun.* **2015**, *66*, 116 – 120.
[45] K. N. Zhang, O. K. Farha, J. T. Hupp, S. T. Nguyen, *ACS Catal.* **2015**, *5*, 4859 – 4866.
[46] L. J. Feng, Q. Chen, J. H. Zhu, D. P. Liu, Y. C. Zhao, B. H. Han, *Polym. Chem.* **2014**, *5*, 3081 – 3088.
[47] S. Fischer, J. Schmidt, P. Strauch, A. Thomas, *Angew. Chem. Int. Ed.* **2013**, *52*, 12174 – 12178; *Angew. Chem.* **2013**, *125*, 12396 – 12400.
[48] M. C. Biesinger, B. P. Payne, A. P. Grosvenor, L. W. M. Lau, A. R. Gerson, R. S. Smart, *Appl. Surf. Sci.* **2011**, *257*, 2717 – 2730.
[49] B. B. Wentzel, P. L. Alsters, M. C. Feiters, R. J. M. Nolte, *J. Org. Chem.* **2004**, *69*, 3453 – 3464.
[50] J. R. L. Smith, Y. Iamamoto, F. S. Vinhado, *J. Mol. Catal. A* **2006**, *252*, 23 – 30.
[51] M. J. Zdilla, J. L. Dexheimer, M. M. Abu-Omar, *J. Am. Chem. Soc.* **2007**, *129*, 11505 – 11511.
[52] C. Arunkumar, Y. M. Lee, J. Y. Lee, S. Fukuzumi, W. Nam, *Chem. Eur. J.* **2009**, *15*, 11482 – 11489.
[53] H. Y. Chen, H. B. Ji, X. T. Zhou, J. C. Xu, L. F. Wang, *Catal. Commun.* **2009**, *10*, 828 – 832.
[54] A. M. d'A. Rocha Gonsalves, A. C. Serra, *J. Chem. Soc. Perkin Trans. 2* **2002**, 715 – 719.
[55] C. J. Liu, W. Y. Yu, C. M. Che, C. H. Yeung, *J. Org. Chem.* **1999**, *64*, 7365 – 7374.
[56] G. A. E. Oxford, M. C. Curet-Arana, D. Majumder, R. W. Gurney, M. L. Merlau, S. T. Nguyen, R. Q. Snurr, L. J. Broadbelt, *J. Catal.* **2009**, *266*, 145 – 155.
[57] L. M. Wilson, A. C. Griffin, *J. Mater. Chem.* **1993**, *3*, 991 – 994.
[58] P. J. F. Gauuan, M. P. Trova, L. Gregor-Boros, S. B. Bocckino, J. D. Crapo, B. J. Day, *Bioorg. Med. Chem.* **2002**, *10*, 3013 – 3021.

Received: April 20, 2016
Published online on ■■ ▮▮, 0000

Homo-heterogeneous POF catalysts: Porous organic framework (POF) materials (PAF-76) with metalloporphyrin components in the frameworks have been prepared by a direct synthesis approach. The as-prepared PAF-76 materials possess three-dimensional conjugated networks, permanent porosity, as well as single and accessible metalloporphyrin active sites. The catalytic properties of PAF-76 catalysts were evaluated for the aerobic oxidation of styrenes, and the catalytic results reveal that PAF-76s exhibit superior performance in terms of high turnover frequency and good product selectivity. The above merits along with the robustness hold great promise for PAF-76 materials in heterogeneous catalysis.

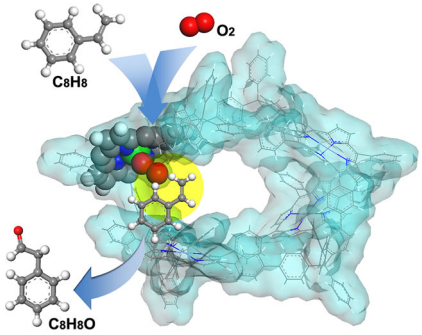

S. Meng, X. Zou, C. Liu, H. Ma, N. Zhao, H. Ren, M. Jia, J. Liu,* G. Zhu*

■■ – ■■

Synthesis and Catalytic Properties of New Metalloporphyrin-Based Porous Organic Framework Materials with Single and Accessible Sites

These are not the final page numbers! ↗↗